processes

MDPI

Article

Evaluation Residual Compressive Strength of Tunnel Lining Concrete Structure after Fire Damage Based on Ultrasonic Pulse Velocity and Shear-Wave Tomography

Qiang Wang [1,*], Daqing Chen [1], Kai Zhu [1], Zitai Zhai [2], Juntao Xu [1], Linlin Wu [1], Dong Hu [3], Weirong Xu [4] and Huandong Huang [5]

[1] College of Quality and Safety Engineering, China Jiliang University, Hangzhou 310018, China; daqingchen97@gmail.com (D.C.); zhukai@cjlu.edu.cn (K.Z.); juntao727209@hotmail.com (J.X.); 14a0604074@cjlu.edu.cn (L.W.)
[2] Jinxi Industries Group Co., LTD, Taiyuan 030027, China; zhaizitai@gmail.com
[3] Taian Special Equipment Inspection and Research Institute, Taian 271099, China; dibiyuhudong@yahoo.com
[4] Huzhou Special Equipment Inspection Center, Huzhou 313099, China; xwr@hztjzx.cn
[5] Ningbo Special Equipment Inspection and Research Institute, Ningbo 315408, China; nbtjyhhd@hotmail.com
* Correspondence: qiangwang@cjlu.edu.cn

Abstract: In this study, ultrasonic pulse velocity (UPV) and ultrasonic shear-wave tomography are combined to measure the residual compressive strength (RCS) of small-scale lining concrete blocks and to detect inner defects in the lining structure. The characteristics of and variations in the RCS of test blocks after being exposed to elevated temperatures (200–800 °C) and constant heating times (2 h, 3 h, and 4 h) were studied. At 800 °C, the RCS values reduced by 64.4%, 69.2%, and 74.6% at heating times of 2 h, 3 h, and 4 h. Scanning electron microscopy (SEM) was used for the micro-phase analysis of the samples that had been exposed to high temperatures. The heating time and RCS as well as the SEM micro-structure relationship were compared. Finally, a tunnel lining slab sample was designed to simulate the post-fire damage inside the blocks. Additionally, shear-wave tomography with 32 probes was able to detect the ϕ10 mm void defects at a depth of 200 mm.

Keywords: concrete lining; fire damage; residual compressive strength; ultrasonic pulse velocity; shear-wave tomography

Citation: Wang, Q.; Chen, D.; Zhu, K.; Zhai, Z.; Xu, J.; Wu, L.; Hu, D.; Xu, W.; Huang, H. Evaluation Residual Compressive Strength of Tunnel Lining Concrete Structure after Fire Damage Based on Ultrasonic Pulse Velocity and Shear-Wave Tomography. *Processes* **2022**, *10*, 560. https://doi.org/10.3390/pr10030560

Academic Editor: Jiaqiang E

Received: 1 February 2022
Accepted: 11 March 2022
Published: 13 March 2022

1. Introduction

Fire accidents in transport tunnels result in severe damage to the tunnel lining because of the high heating rates and elevated temperature exposure that take place during fires [1–3]. When the concrete lining of a tunnel is exposed to fire, the chemical composition and physical structure change, resulting in a significant reduction in the strength, modulus of elasticity, and volume stability of the lining [4,5]. These losses in the materials comprising lining concrete during the early stages of heat exposure and the concrete that falls of due to prolonged heat exposure results in material loss [6].

Tunnel linings can suffer heavy structural damage or even collapse when exposed to fire over a long period of time. An assessment of post-fire damage is the most important thing when evaluating the structural safety of a tunnel's concrete lining. There are several examples of fires that have resulted in severe damage to the concrete linings of tunnels, resulting in the tunnels having serious concrete spalling problems [7].

Full-scale experimental tests were conducted on TBM (tunnel boring machine) tunnel linings exposed to standard high temperatures (0–600 °C), and the behavior of the concrete lining segments was analyzed [8,9]. Fire damage imparted to a tunnel liner is characterized using temperature criteria and structural response [10]. A combination of influencing factors were evaluated using static loading tests to evaluate that fire damage imparted to the tunnel linings [11]. The thermal and spalling behaviours of fire-resistant

concrete tunnel lining segments were analyzed [12]. Above studies were dependent on the mechanical compression test of the samples or the drilling core taking place on-site. In tunnels especially, there are problems related to obtaining core samples [13]. These concrete lining sample measurement methods are destructive testing methods.

Ultrasonic pulse velocity (UPV) is a typical nondestructive testing (NDT) method that is dependent on the concrete's elastic properties and the density of the concrete. UPV was developed to reveal the tunnel lining structure of fire damaged concrete [12]. The propagation velocity of longitudinal and transverse ultrasonic waves is related to the degree of degradation in the concrete's compressive strength after a fire [14–16]. The relationship between compressive strength and UPV propagation has been analyzed [17–19]. Recently, the UPV has been used to quantitatively evaluate the residual compressive strength (RCS) of concrete that has been subjected to elevated temperatures ranging from 400 to 600 °C [20] Concrete specimens were heated at temperatures ranging from 400 to 1000 °C, and the relationship between RCS and UPV was investigated [21]. After fire damage the use of UPV for the assessment of the RCS of concrete is one of the most interesting subjects in the field of NDT and reveals the extent of fire damage in concrete [22,23]. The developed wave velocity ratio measured using the ultrasonic pulse technique and artificial intelligence can be used to identify the degree and of thermally induced damage in concrete [24]. The possibility of using different regression models to predict the mechanical properties of limestone concrete, self-compacting glass concrete and eco-concretes with fine and coarse after exposure to high temperatures were discussed based on UPV [25–27].

Furthermore, other NDT schemes, such as the seismic method (refraction) and GPR data, have been combined to characterize the fire damage incurred to the concrete of tunnel walls [28]. The evaluation of the residual tensile strength of fire-damaged concrete using a non-linear resonance vibration method was proposed [29]. A tricolor image processing method was proposed to analyze the color changes in the concrete lining of tunnels and to evaluate the damage caused by fire [30]. UPV is the most promising NDT method that has been used to establish an accurate relationship between the RCS and the UPV propagation in concrete after exposure to elevated temperatures. The continuous heating of the lining structure and hence the stiffness and strength degradations in the lining materials are obvious.

Though the RCS of concrete tunnel lining can be examined with NDT methods, the damage (voids, cracks) inside a lining layer that has been subjected to elevated temperatures is also indispensable for safety assessments. Ultrasonic shear-wave tomography with multiple arrays of probes (commonly known as MIRA) overcomes the limitations of conventional ultrasonic testing methods [31] and could be an ideal NDT method for the evaluation of post-fire concrete integrity. MIRA was able to accurately detect horizontal cracks or delamination in continuously reinforced concrete [32]. The multi-layer delay-and-sum method was combined with a synthetic aperture focusing technique to develop an ultrasonic imaging method for multi-layer concrete structures based on MIRA [33], a 2D full-waveform inversion of ultrasonic waves for delamination and rebar debonding detection in concrete structures [34]. MIRA is also a promising method for the inspection of post-fire damage in concrete linings.

The objectives of this paper are to find an ultrasonic NDT method (combined UPV and ultrasonic array tomography) for the post-fire detection of RCS and inside damage in concrete linings. Focusing on the constant heating time, a model combining the RCS and UPV of tunnel lining samples under elevated temperatures (200 to 800 °C) was built to evaluate fire damage. In an in-field tunnel case, MIRA was used to evaluate the simulated defects inside of a concrete lining slab.

2. Materials and Methods

2.1. UPV Test and Shear-Wave Tomography Equipment

The test concrete specimens used for furnace testing were small 150 × 150 × 150 mm blocks based on standard code GB 50010-2010 [35]. Ordinary 32.5R Portland cement, a

coarse aggregate of crushed stone with an average particle size of 30 mm, a fine aggregate of yellow sand (coarse sand), and tap water were used as raw materials. The mix ratio of the cement determining the composition of the concrete block was as follows: cement: water: sand: stone = 1:0.45:1.36:3.03. The compressive strength of the concrete lining sample was 30–35 MPa (model C30). After being casted for 16 h, all of the blocks were demolded and placed in a curing room at a temperature of 20 ± 2 °C and a relative humidity of more than 90%. The curing time was 28 days.

The YFFG10/12Q-YC model furnace used in the present study has a chamber size of 200 mm × 200 mm × 250 mm, as shown in Figure 1a, and the elevated temperatures varied from 200 °C to 800 °C. Heating rate was 10 °C/min up to the target temperature. The peak temperature was maintained for a period of 2, 3, and 4 h (constant heating time). A cooling rate of 8 °C/min was applied, and the samples were then allowed to cool gradually at air at room temperature [36].

(**a**) Furnace.

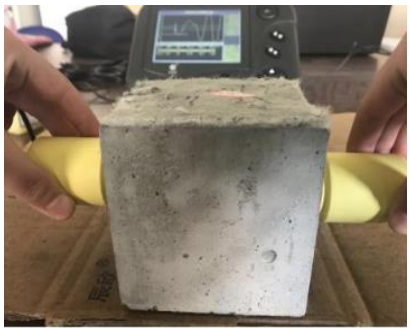

(**b**) Ultrasonic pulse transmission time measurement.

(**c**) Compressive testing machine.

Figure 1. The experimental set-up.

A transmitted ultrasonic pulse frequency 50 kHz was applied, and pulse transmission time was measured as shown in Figure 1b. An NM-4A non-metal ultrasonic wave detector from Beijing concrete engineering Corp was chosen for the UPV test. The transmission times of the ultrasonic pulse through the unexposed blocks and fire-exposed blocks were compared. Each point was tested three times. The measured ultrasonic wave transmission time Δt through the block was used to calculate the pulse velocity v. Finally, the compressive tests were conducted using an MTS servo-hydraulic universal testing machine with a capacity of 2000 kN, as seen in Figure 1c. The cubic block was axially loaded at 0.5 MPa/s post-fire exposure. Typical concrete specimens were tested under different elevated temperatures, as seen in Figure 2. MIRA is a low frequency (20–100 kHz) multifunctional phased array ultrasonic system that can be used to detect objects, interfaces, and anomalies in concrete structures [30]. Since the ultrasonic probes in MIRA do not require a coupling gel to ensure the transmission of waves into the concrete, the probe can be moved from one position to the next position with almost no surface preparation. Shear wave velocity is 2160 m/s. MIRA-A1020 consists of 32 dry-point-contact (DPC) transmitting and receiving transducers in a matrix antenna array with 8 channels spaced 30 mm apart; each channel has four transducers that are laterally spaced 25 mm apart. If each channel acts as either a transmitter or a receiver, then there are a total of 56 transmitting and receiving pairs for 8 channels. One of the most powerful features of MIRA is its ability to reconstruct the condition of concrete in a three-dimensional format. The MIRA-A1020 set-up is shown in Figure 3.

Figure 2. Typical test blocks under exposed temperatures (200 to 800 °C).

Figure 3. MIRA A1020 set-up.

2.2. SEM Analyses

Microstructural analyses of the concrete specimens were carried out using a scanning electron microscope (SEM). A TM-3000 Hitachi scanning electron microscope was used after a uniaxial compression test was carried out on the specimens. The samples were less than 4 mm in size. SEM investigations of linings of the concrete blocks showed that obvious changes had happened at the micro-scale of exposure to elevated temperatures.

3. Results and Discussion

3.1. UPV and Constant Heating Time

The ultrasonic pulse velocity was measured through blocks comprising the heat-exposed test specimens. At room temperature (25 °C), the average UPV of the test blocks was 3850 m/s, and the initial compressive strength was 31.5 MPa. When the temperature was elevated to 200 °C, the v was 3810 m/s, and the compressive strength was 29.3 MPa. As such, when the temperature changes from 25 °C to 200 °C, the variations in velocity and compressive strength values are not obvious. Because of this, the specimens under the temperature exposure range from 200 °C to 800 °C are focused on instead. To investigate the relative increase in the pulse transmission time after exposure to elevated temperatures (200–800 °C), the linear fitting lines of the UPV and temperature under constant heating times (2 h, 3 h and 4 h) are presented in Figure 4. For the heating times of 2 h, 3 h, and 4 h, the three equations are as follows:

$$T = 4.87 - 0.004v \quad (1)$$

$$T = 4.66 - 0.005v \quad (2)$$

$$T = 4.25 - 0.005v \quad (3)$$

In Equations (1)–(3), T is the elevated temperature, and v is ultrasonic velocity. The fitting line R values are 0.97, 0.96, and 0.96, respectively. Concrete that has been exposed high temperature has a linear relationship with velocity. For the same heating exposure time, the ultrasonic wave velocity decreases when the temperature is elevated to the 200 °C–800 °C range. For the constant heating time of 2 h, the ultrasonic wave velocity of the 600 °C specimen reduced by about 45%, compared to that of the 400 °C specimen. For a constant heating time of 4 h, the value of v reduced by about 32% when the temperature changed from 400 °°C to 600 °C. Therefore, the constant heating time had a limited effect on the variations in the specimens' velocities.

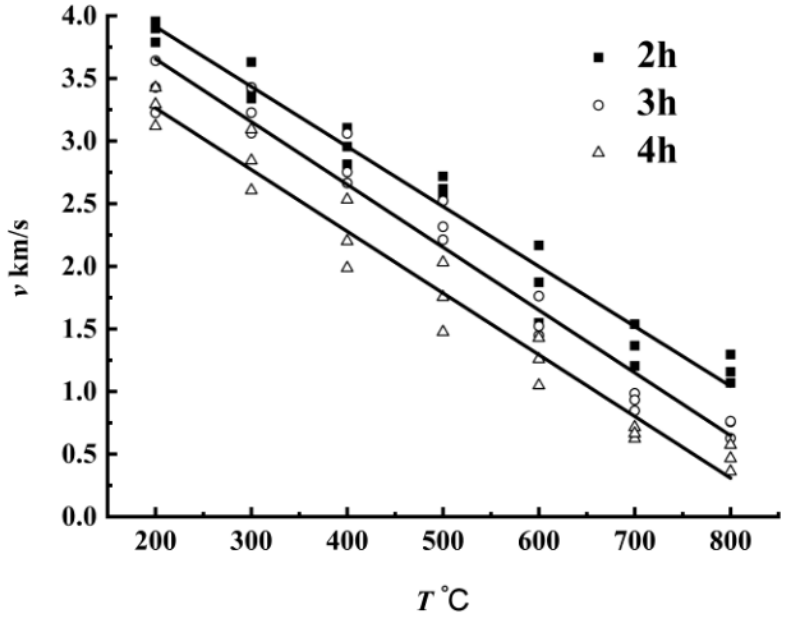

Figure 4. Velocity vs. temperature under different heating times.

The relationship between RCS and the elevated temperature of the concrete specimen has been studied previously [1,8,20]. The relationship between the RCS and elevated temperature under constant heating times (2 h, 3 h and 4 h) was analyzed in this study. The concrete blocks underwent eight temperature series ranging from 200 °C to 800 °C in the compressive test. Each series consisted of three cubic blocks to be tested with the MTS

servo-hydraulic testing machine. During the hydraulic test, three sets of lining concrete specimens were placed under different exposure temperatures and maintained at different heating times for 2 h, 3 h, and 4 h. The regression curves are compared in Figure 5. The fitting curve equations for the exposure times of 2 h, 3 h, and 4 h are

$$f_{cu} = 9.39v_2^{0.81} \quad (4)$$

$$f_{cu} = 10.81v_3^{0.70} \quad (5)$$

$$f_{cu} = 11.23v_4^{0.71} \quad (6)$$

where v_2, v_3, and v_4 are the average ultrasonic wave velocity under the heating times of 2 h, 3 h, and 4 h, and f_{cu} is the RCS value. The correlation coefficients R are 0.92, 0.90, and 0.96, respectively. As such, it is viable to use velocity v to measure the f_{cu} after fire exposure.

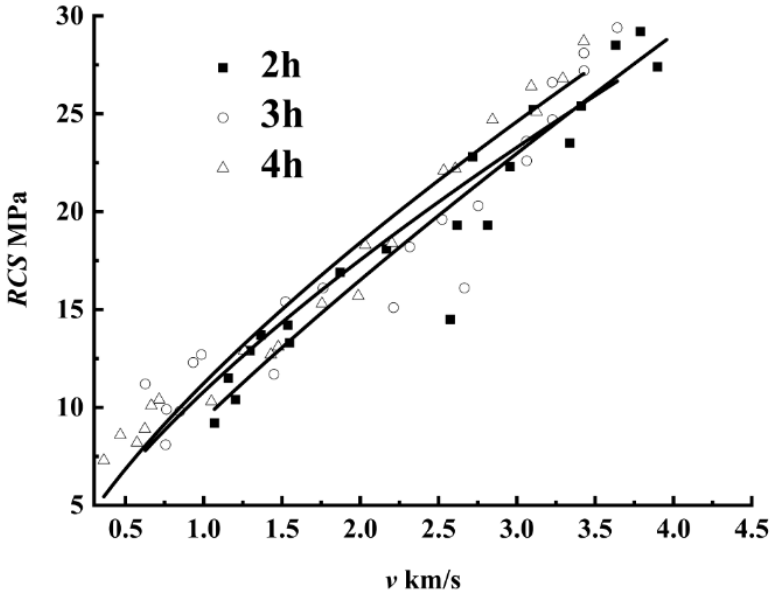

Figure 5. RCS vs. velocity under different heating times.

Then, the f_{cu} values are compared at the constant heating times of 2 h, 3 h, and 4 h constant in Figure 6. For the fixed exposure heating times (2 h, 3 h or 4 h), it is clear that variations in the f_{cu} values have the same trend. For the defined temperature, three f_{cu} of the heating time (2 h, 3 h or 4 h) values are nearly stable. The f_{cu} reduction trend is obvious as the temperature increases. At 200 °C, the f_{cu} value reduces by about 12%~20%, compared to at room temperature. Due to free water evaporation, cracks and voids were produced in the inner part of the concrete. At 400 ºC, f_{cu} the value reduces by 38%~50% compared to the f_{cu} value at room temperature. At 600~800 °C, the f_{cu} value reduces slowly, and f_{cu} value decreases by about 3%~9% for each 100 °C increase. At 800°C, there was loss in the f_{cu} value of about 70%.As the constant heating time (2 h, 3 h, and 4 h) increased, the variations in the RCS maintained a decreasing trend. The mean f_{cu} values are 28.0 MPa, 25.0 MPa, 20.3 MPa, 17.4 MPa, 14.2 MPa, 11.4 MPa, and 9.6 MPa under 200~800 °C, respectively, and the corresponding max-deviations are 2.2 MPa, 1.4 MPa, 3.6 MPa, 3.3 MPa, 4.1 MPa, 3.0 MPa, and 3.2 MPa.

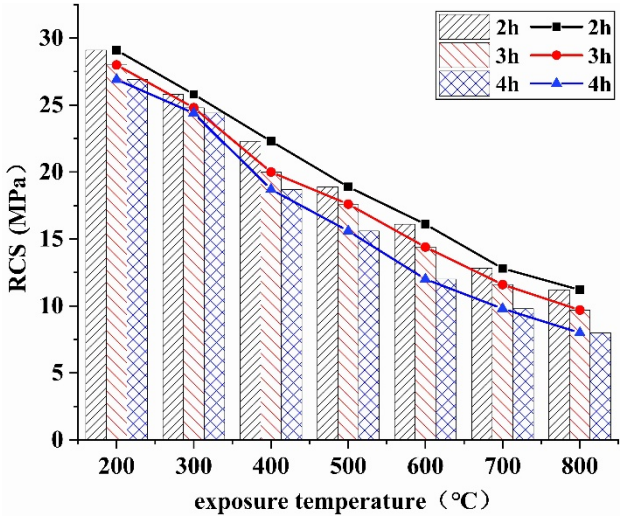

Figure 6. RCS vs. temperature under constant heating times.

3.2. Post-Fire Specimen Micro-Phase Analyses

A number of chemo-physical properties are markedly affected by exposure to high temperatures of 200 °C–800 °C (density of micro-cracks, porosity, humidity, chemical composition, etc.) The typical concrete matrix materials, cement paste, the paste–aggregate interface area micro-phase characteristics are compared in SEM images with a 3 h exposure hold time in Figure 7.

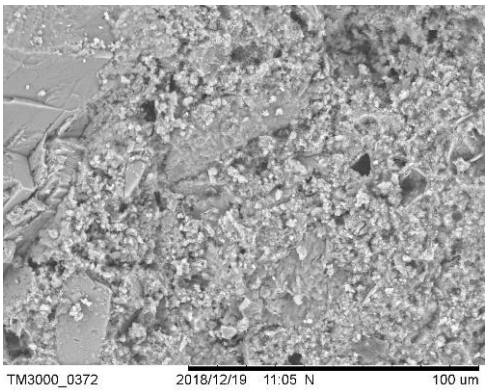

(**a**) 200 °C exposed sample.

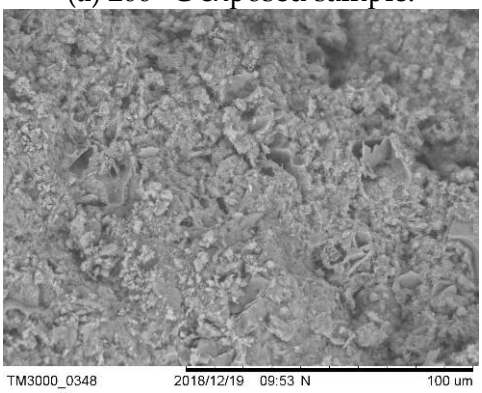

(**b**) 400 °C exposed sample.

Figure 7. *Cont.*

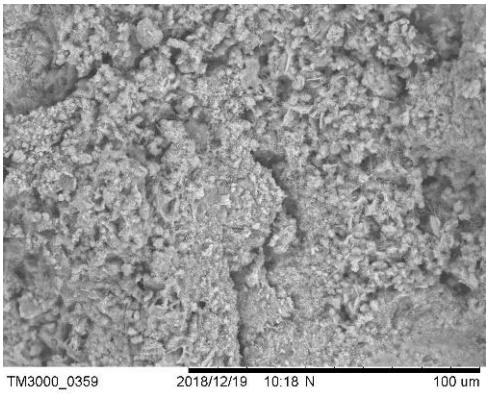

(**c**) 600 °C exposed sample.

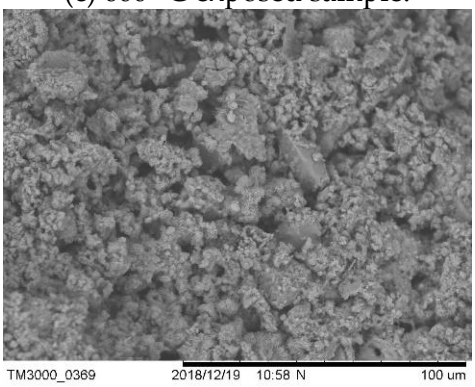

(**d**) 800 °C exposed sample.

Figure 7. The SEM images of samples exposed at temperatures of 200 °C–800 °C.

From the SEM image of the 200 °C exposed specimen in Figure 7a, the hydration products of the cement paste structure are complete. There is a large amount of tight C-S-H gel, but some micro-cracks and portlandite $Ca(OH)_2$ particles can be observed. The structure of the hydration product is normal. Some crystal water has evaporated.

In the specimen exposed to 400 °C, as seen in Figure 7b, the changes emerged in the cement paste and aggregate interfaces, and the structure became looser. This led to a thermal decohesion of the aggregate particles. Some micro-cracks appeared in the Portland hydrate, and the gel porosity increased. Due to crystallization and free water evaporation, the hydration products were decomposed. The ettringite (AFt) crystals were completely dehydrated. The C-H crystals had reduced compared to in the SEM image of the 200 °C sample. The structure between the phases is loose and not tight, resulting in a small number of micro-cracks. The surface of the aggregate is smooth and flat, and it has peeled off from the hydration product.

In Figure 7c, the aggregate–paste interface area of the cement paste and aggregate shows distinct cracks on the surface under 600 °C. In the SEM-observed area, there are no layer-structured $Ca(OH)_2$ crystals. The cracks on the sample surface were caused by burst as a result of the internal pressure.

The specimen's microstructure when the exposure temperature reached 800 °C is shown in Figure 7d. The cement paste structure looked like honeycomb. The cement paste and aggregate interface area had cracks and holes. The hydrates had decomposed completely. The C-S-H glue was dehydrated, and the damage was in a discontinuity state. The $CaCO_3$ had decomposed quickly, and the strength of the inner structure strength had greatly reduced. Fire caused serious damage to the lining concrete. On the whole, the 400 °C exposure temperature is the turning point at which the RCS value decreased. The cohesive force between the aggregate and cement mortar decreased, and cracks had started to appear on the surface of the specimen and parts had started falling off.

3.3. Microstructure and Constant Heating Time

When the exposure temperature reached 400 °C, different exposure heating times (2 h, 3 h, and 4 h) were set for the specimens. The microstructures of the specimens when different constant heating temperatures were maintained are compared in Figure 8. In Figure 8a, when the exposure heating time was 2 h, the internal structure of the concrete was still connected, but the hydration products began to become looser. The net-like structure of C-S-H gel also started to decompose. It can be seen in Figure 8b that when the exposure heating time is 3 h, the overall structure of the cement paste and the microstructure change significantly. A porous structure emerged in the cement, and it became looser overall. At this stage, a large amount of crystalline water evaporated, which caused obvious voids to be produced on the C-S-H gel surface. In Figure 8c, when the exposure heating time was 4 h, the morphology of the C-S-H gel in the entire microstructure takes on a velutinous shape due to the gradual decomposition of the C-S-H gel. No complete Ca $(OH)_2$ is present. The water absorbed by CaO in the air causes the volume of the whole structure to increase, and the internal structure of the test block is seriously damaged.

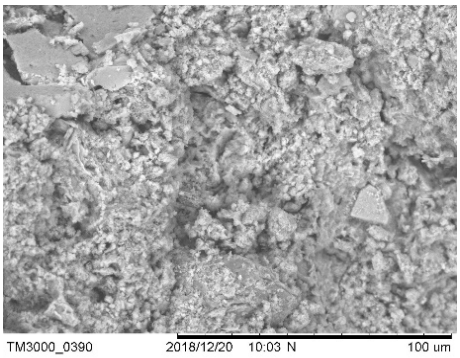

(**a**) 2h

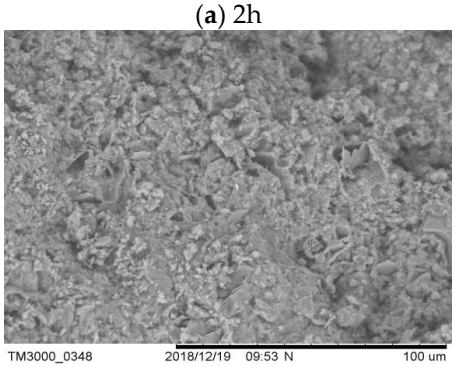

(**b**) 3h

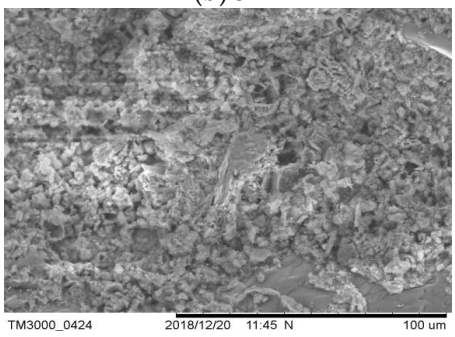

(**c**) 4h

Figure 8. Typical exposure temperature of 400 °C after 2 h, 3 h, and 4 h of heating time.

3.4. Concrete Lining Shear-Wave Tomography

The concrete lining test site was located in the Zhijing tunnel, Hangzhou City, seen in Figure 9. The concrete lining slab was 1000 × 800 × 200 mm in size. The similar-sized specimen of the tunnel lining concrete slab was designed for inner defect detection and can be seen in Figure 10.

Figure 9. Tunnel site and tunnel lining structure.

Figure 10. Schematic grid of the testing slab.

Based on the grid in Figure 10, each ultrasonic test provided an individual B-scan. After all of the B-scan results were fused, the slice in the transverse direction of the equipment provides a 3D view of the sample damage. In Figure 11a, the focused image has an apparent depth 210 mm, which is different from the actual bottom depth of 200 mm. The location error is about 10 mm. The focused images that were obtained using SAFT illustrated the existence of simulated fire damage inside the concrete lining. The four red dots at the upper portion of the screen indicate two voids (ϕ10 mm, ϕ30 mm) and two rebars (ϕ20 mm, ϕ10 mm). In Figure 11a, in the B-scan image from left to right, the depth of the voids and rebar are 93 mm, and the location error is −7 mm. It is in the accepted error range. In Figure 11b, which shows a C-scan image, a ϕ10 mm rebar and ϕ20 mm, ϕ10 mm, and ϕ30 mm voids, and the diameters are 27 mm, 35 mm, 20 mm, and 40 mm, respectively. The location errors are +17 mm, +15 mm, +10 mm, and +10 mm. Though the depth location errors are not small due to heterogeneities in the concrete structure, they also supply rich information about the lining inner structure. A 3D-scan view of the concrete slab is shown in Figure 11c. MIRA was able to detect the diameter of a ϕ10 mm void and to detect defects at the depths of 100 and 200 mm. These findings meet requirements for concrete lining structure inner defect inspection. The other red dots (clutters) indicate small cracks or voids inside the specimen, which indicate poor concrete consolidation or contamination.

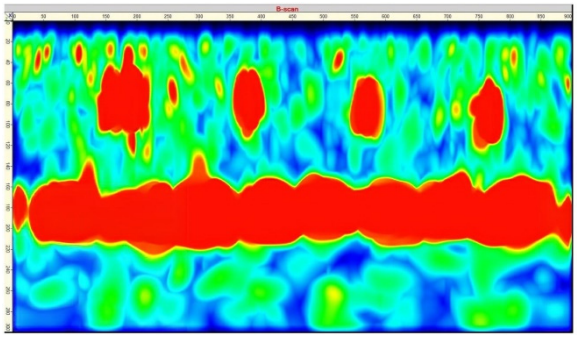

(**a**) B-scan view.

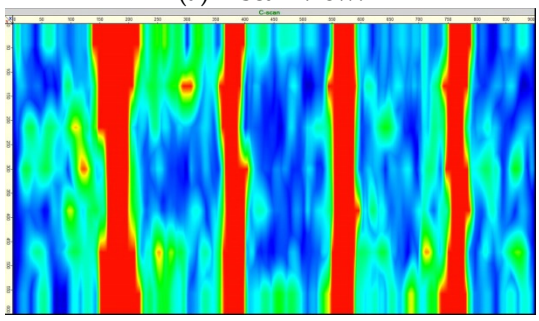

(**b**) C-scan view.

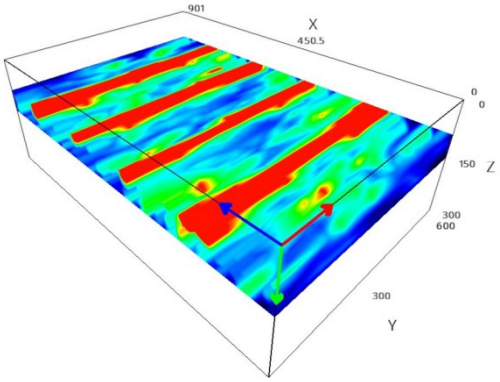

(**c**) 3D-scan view.

Figure 11. Illustrations of ultrasonic imaging test: (**a**) B-scan, (**b**) C-scan, (**c**) 3D-scan.

4. Conclusions

In this study, UPV and ultrasonic shear-wave tomography were first combined to measure the RCS of tunnel-lining concrete blocks and to detect the inner defects of the lining structure. Small-scale 150 × 150 × 150 mm concrete blocks were heated to analyze the variation between RCS and UPV under elevated temperatures (200–800 °C) and at constant heating times (2 h, 3 h and 4 h). The outcomes of the concrete lining tests demonstrated that the RCS has a nearly linear relationship with the ultrasonic pulse velocity when subjected to elevated temperatures (200–800 °C). The *R* value was larger than 0.95. At 800 °C, the RCS values reduced by 64.4%, 69.2%, and 74.6% at the constant heating times of 2 h, 3 h, and 4 h compared to the initial value. The velocity is sensitive to the elevated temperature of the lining concrete after exposure to different heating times. The micro-phase SEM structure images validated the failure of the inner structure of the test blocks at elevated temperatures. A tunnel lining slab that was similar in size was designed to inspect the simulated damage after fire exposure using MIRA. The 3D ultrasonic views supply precise information about specimen's simulated inner defects (voids, rebars). The experimental results provide a reference for the assessment of post-fire tunnel-lining concrete damage.

Author Contributions: Conceptualization, Q.W. and J.X.; methodology, D.C. and K.Z.; software, L.W.; validation, Z.Z. and D.H.; data curation, W.X.; writing—original draft preparation, Q.W., Z.Z. and H.H. All authors have read and agreed to the published version of the manuscript.

Funding: This work was supported by the "Pioneer" and "Leading Goose" R&D Program of Zhejiang under Grant 2022C03179 and the Key Research and Development Project of Zhejiang Province under grant 2018C03029.

Institutional Review Board Statement: Not applicable.

Informed Consent Statement: Not applicable.

Data Availability Statement: Not applicable.

Conflicts of Interest: There are no conflicts of interest.

References

1. Savov, K.; Lackner, R.; Mang, H.A. Stability assessment of shallow tunnels subjected to fire load. *Fire Saf. J.* **2005**, *40*, 745–763. [CrossRef]
2. Faure, R.M.; Karray, M. Investigation of the concrete lining after the Mont Blanc tunnel fire. *Struct. Eng. Int.* **2007**, *2*, 123–132. [CrossRef]
3. Sakkas, K.; Vagiokas, N.; Tsiamouras, K.; Mandalozis, D.; Benardos, A.; Nomikos, P. In-situ fire test to assess tunnel lining fire resistance. *Tunn. Undergr. Space Technol.* **2019**, *85*, 368–374. [CrossRef]
4. Albrektsson, J.; Flansbjer, M.; Lindqvist, J.E.; Jansson, R. *Assessment of Concrete Structures after Fire*; SP Technical Research Institute of Sweden: Borås, Sweden, 2011.
5. Oneschkow, N. Fatigue behaviour of high-strength concrete with respect to strain and stiffness. *Int. J. Fatigue* **2016**, *87*, 38–49. [CrossRef]
6. Sýkora, J.; Jarušková, D.; Šejnoha, M.; Šejnoha, J. Fire risk analysis focused on damage of the tunnel lining. *Fire Saf. J.* **2018**, *95*, 51–65. [CrossRef]
7. Boström, L.; Larsen, C.K. Concrete for tunnel linings exposed to severe fire exposure. *Fire Technol.* **2006**, *42*, 351–362. [CrossRef]
8. Yan, Z.G.; Zhu, H.H.; Ju, J.W.; Ding, W.Q. Full-scale fire tests of RC metro shield TBM tunnel linings. *Constr. Build. Mater.* **2012**, *36*, 484–494. [CrossRef]
9. Yan, Z.G.; Zhu, H.H.; Ju, W.J. Behavior of reinforced concrete and steel fiber reinforced concrete shield TBM tunnel linings exposed to high temperatures. *Constr. Build. Mater.* **2013**, *38*, 610–618. [CrossRef]
10. Hua, N.; Tessari, A.; Khorasani, N.E. Characterizing damage to a concrete liner during a tunnel fire. *Tunn. Undergr. Space Technol.* **2021**, *109*, 103761. [CrossRef]
11. Hua, N.; Khorasani, N.E.; Tessari, A.; Ranade, R. Experimental study of fire damage to reinforced concrete tunnel slabs. *Fire Saf. J.* **2022**, *127*, 103504. [CrossRef]
12. Alhawat, H.; Hamid, R.; Baharom, S.; Azmi, M.R.; Kaish, A.B.M.A. Thermal behaviour of unloaded concrete tunnel lining through an innovative large-scale tunnel fire experimental testing setup. *Constr. Build. Mater.* **2021**, *283*, 122718. [CrossRef]
13. Felicetti, R. Assessment methods of fire damages in concrete tunnel linings. *Fire Technol.* **2013**, *49*, 509–529. [CrossRef]
14. Qiao, R.; Shao, Z.; Liu, F.; Wei, W. Damage evolution and safety assessment of tunnel lining subjected to long-duration fire. *Tunn. Undergr. Space Technol.* **2019**, *83*, 354–363. [CrossRef]
15. Hwang, E.; Kim, G.; Choe, G.; Yoon, M.; Gucunski, N.; Nam, J. Evaluation of concrete degradation depending on heating conditions by ultrasonic pulse velocity. *Constr. Build. Mater.* **2018**, *171*, 511–520. [CrossRef]
16. Silva, F.A.N.; Nogueira, C.L.; Silva, J.A.; Araújo, A.V.; Azevedo, A.J.; Delgado, J.M.P.Q. Ultrasonic assessment of damage in concrete under compressive and thermal loading using longitudinal and transverse waves. *Russ. J. Nondestruct.* **2019**, *55*, 808–816. [CrossRef]
17. Bogas, J.A.; Gomes, M.G.; Gomes, A. Compressive strength evaluation of structural lightweight concrete by non-destructive ultrasonic pulse velocity method. *Ultrasonics* **2013**, *53*, 962–972. [CrossRef] [PubMed]
18. Ghosh, R.; Sagar S, P.; Kumar, A.; Gupta, S.K.; Kumar, S. Estimation of geopolymer concrete strength from ultrasonic pulse velocity (UPV) using high power pulser. *J. Build. Eng.* **2018**, *16*, 39–44. [CrossRef]
19. Al-Nu'man, B.S.; Aziz, B.R.; Abdulla, S.A.; Khaleel, S.E. Compressive strength formula for concrete using ultrasonic pulse velocity. *Int. J. Eng. Trends Technol.* **2015**, *26*, 9–13. [CrossRef]
20. Yang, H.; Lin, Y.; Hsiao, C.; Liu, J.Y. Evaluating residual compressive strength of concrete at elevated temperatures using ultrasonic pulse velocity. *Fire Saf. J.* **2009**, *44*, 121–130. [CrossRef]
21. Lin, Y.; Hsiao, C.; Yang, H.; Lin, Y. The effect of post-fire-curing on strength-velocity relationship for nondestructive assessment of fire-damaged concrete strength. *Fire Saf. J.* **2011**, *46*, 178–185. [CrossRef]
22. Iqbal, H.W.; Khushnood, R.A.; Baloch, W.L.; Nawaz, A.; Tufail, R.F. Influence of graphite nano/micro platelets on the residual performance of high strength concrete exposed to elevated temperature. *Constr. Build. Mater.* **2020**, *253*, 119029. [CrossRef]

23. Abed, M.; Brito, J.D. Evaluation of high-performance self-compacting concrete using alternative materials and exposed to elevated temperatures by non-destructive testing. *J. Build. Eng.* **2020**, *32*, 101720. [CrossRef]
24. Chen, L.-H.; Chen, W.-C.; Chen, Y.-C.; Lin, H.-J.; Cai, C.-F.; Lei, M.-Y.; Wang, T.-C.; Hsu, K.-W. Using Ultrasonic Pulse and Artificial Intelligence to Investigate the Thermal-Induced Damage Characteristics of Concrete. *Appl. Sci.* **2018**, *8*, 1107. [CrossRef]
25. Blumauer, U.; Hozjan, T.; Trtnik, G. Prediction of mechanical properties of limestone concrete after high temperature exposure with artificial neural networks. *Adv. Concr. Constr.* **2020**, *10*, 247–256.
26. Ling, T.C.; Poon, C.S.; Kou, S.C. Influence of recycled glass content and curing conditions on the properties of self-compacting concrete after exposure to elevated temperatures. *Cem. Concr. Compos.* **2012**, *34*, 265–272. [CrossRef]
27. Velay-Lizancos, M.; Martinez-Lage, I.; Azenha, M.; Vázquez-Burgo, P. Influence of temperature in the evolution of compressive strength and in its correlations with UPV in eco-concretes with recycled materials. *Constr. Build. Mater.* **2016**, *124*, 276–286. [CrossRef]
28. Abraham, O.; Dérobert, X. Non-destructive testing of fired tunnel walls: The Mont-Blanc Tunnel case study. *NDT&E Int.* **2003**, *36*, 411–418.
29. Park, S.J.; Yim, G.K.; Hong, J.; Kwak, H.G. Evaluation of residual tensile strength of fire-damaged concrete using a non-linear resonance vibration method. *Mag. Concrete Res.* **2015**, *67*, 235–246. [CrossRef]
30. Du, S.; Zhang, Y.; Sun, Q.; Gong, W.; Geng, J.; Zhang, K. Experimental study on color change and compression strength of concrete tunnel lining in a fire. *Tunn. Undergr. Space Techol.* **2018**, *71*, 106–114. [CrossRef]
31. Aldo, O.; Samokrutov, A.A.; Samokrutov, P.A. Assessment of concrete structures using the Mira and Eyecon ultrasonic shear wave devices and the SAFT-C image reconstruction technique. *Constr. Build. Mater.* **2013**, *38*, 1276–1291.
32. Choi, P.; Kim, D.H.; Lee, B.H.; Won, M.C. Application of ultrasonic shear-wave tomography to identify horizontal crack or delamination in concrete pavement and bridge. *Constr. Build. Mater.* **2016**, *121*, 81–91. [CrossRef]
33. Lin, S.; Shams, S.; Choi, H.; Azari, H. Ultrasonic imaging of multi-layer concrete structures. *NDT&E Int.* **2018**, *98*, 101–109.
34. Chen, R.; Tran, K.T.; La, H.M.; Rawlinson, T.; Dinh, K. Detection of delamination and rebar debonding in concrete structures with ultrasonic SH-waveform tomography. *Autom. Constr.* **2022**, *133*, 104004. [CrossRef]
35. *GB 50010-2010*; Code for Design of Concrete Structure. Ministry of housing and Urban-Rural Development of P.R. China: Beijing, China, 2010.
36. Zhai, Z.T. Ultrasonic Testing and Experimental Study on Damage of Lining Structure Concrete after Tunnel Fire. Master's Thesis, China Jiliang University, Hangzhou, China, 2020.